Modeling incoherent reflections from rough room surfaces with image sources

Samu Siltanen,[a] Tapio Lokki, Sakari Tervo, and Lauri Savioja
Department of Media Technology, Aalto University School of Science, P.O. Box 15400, FI-00076 Aalto, Finland

(Received 22 December 2011; revised 10 April 2012; accepted 10 April 2012)

Reflections at rough surfaces change the temporal structure of the reflected signal. This paper shows how to incorporate this temporal behavior in geometric room acoustics modeling. Specifically, a beam tracer is used for calculating the image sources and reflection paths. The roughness of the surfaces is taken into account in post-processing. A single reflection is assumed to distribute the energy according to an exponential function in time based on Biot's rough surface modeling theory. Multiple reflections are modeled with convolutions of exponential functions which are approximated as gamma functions. © *2012 Acoustical Society of America*.
[http://dx.doi.org/10.1121/1.4711013]

PACS number(s): 43.55.Ka, 43.55.Br, 43.20.Dk [NX] Pages: 4606–4614

I. INTRODUCTION

Specular reflections are widely used in room acoustic modeling algorithms to model the interaction of sound waves and room surfaces. The assumption of specular reflections is valid when the surfaces are smooth. However, in reality, room surfaces are often rough. Thus, the reflected sound is spread, not only spatially, but also in time. Such reflections are incoherent, since the phase and temporal envelope are not preserved at the reflection. Lokki *et al.* (2011) have shown that there is a significant perceptual difference between coherent (specular) reflections and incoherent reflections.

In geometric room acoustics modeling, scattering from rough surfaces is often modeled by using a random-incident scattering coefficient (see definition in Vorländer and Mommertz, 2000 or Cox *et al.*, 2006). Sound energy is sent in other than specular direction in the proportion determined by that coefficient (see, i.e., Dalenbäck, 1996). While this approach might be sufficient for modeling the spatial spreading of sound, it is insufficient for modeling the temporal spreading. Reflection via a single rough surface produces single peak in a response. The rough surface must be divided into several pieces to yield multiple peaks or a temporally spread response. This, in most cases, violates the assumption of geometric acoustics that the modeled wavelength must be much less than the dimensions of the details.

It is possible to model the incoherent reflections by using a digital filtering approach as in Huopaniemi *et al.* (1997) and design a frequency-dependent filter for each material (see, e.g., Savioja *et al.*, 1999). However, there is no obvious way to combine the effects of several sequential reflections because it requires either applying filters multiple times per reflection path or designing separate filters for each combination of materials.

This paper presents one way to introduce incoherent reflections in a beam tracer algorithm. It is assumed that $ka \ll 1$, where a is a typical dimension of the roughness and k is the wave number. The presented technique allows using large surfaces in the modeling as assumed in geometric acoustics. It also provides a simple formulation for the time spreading behavior of rough surfaces that makes it easy to combine multiple reflections.

A. Previous work

In areas other than room acoustics, there are several approaches to modeling reflections from rough surfaces, each of which makes different assumptions. Rayleigh (1945) modeled corrugated surfaces with a periodic sinusoidal function. Perturbation techniques model the roughness as perturbations of a smooth plane and require that the height deviations are small compared to the modeled wavelength, and that the gradient is small (see, e.g., Gilbert and Knopoff, 1960). The Kirchhoff approximation assumes that the surface is sufficiently smooth so that there is no self-shadowing and a reflection from a point can be approximated with a reflection from its tangent plane (see, e.g., Eckart, 1953). Basically, this means that the surface gradient must not change too rapidly. An interested reader is advised to refer to Ogilvy (1987) for more information.

In their basic forms, neither perturbation technique nor Kirchhoff approximation take into account shadowing or multiple scattering by different parts of the rough surface, which is often the case in room acoustics. Thus, in this paper, a model suggested by Twersky (1957) is chosen since it accounts for these phenomena. This model is applicable to all frequencies and it is in agreement with measurement data as shown by Chu and Stanton (1990), although it is sensitive to the surface parameters used.

The model was further developed by Biot (1957, 1958, 1968) and Tolstoy (1979, 1981, 1984). With the assumption that the roughness dimensions are much smaller than the modeled wavelength, the theory allows replacing the roughness with a simple linear boundary condition for the wave equation

[a]Author to whom correspondence should be addressed. Electronic mail: Samuel.Siltanen@tml.hut.fi

 0001-4966/2012/131(6)/4606/9/$30.00

$$\frac{\partial^2\phi}{\partial x^2}+\frac{\partial^2\phi}{\partial y^2}+\frac{\partial^2\phi}{\partial z^2}+k^2\phi=0, \tag{1}$$

at a corresponding smooth surface, $z=0$, and it implicitly models interaction between different parts of the surface. The velocity potential is denoted with ϕ and $k=2\pi f/c$ is the wave number for frequency f and speed of sound c.

The first model by Biot (1957, 1958) models the rough surface as a distribution of hemispherical bosses on a flat surface. Although this model is not very realistic for most rough surfaces, it provides an interesting insight. The rough surface can be modeled with a distribution of dipoles on the surfaces. Biot provides equations for the dipoles depending on the boss size and density. The dipole distribution can then be represented with a distribution of image sources on a line perpendicular to the surface and below the flat surface image source. The amplitudes of those image sources decay exponentially along the depth.

Later, in Biot (1968), the model was extended to more general types of rough surfaces. The generalized model includes boundary conditions for various shapes of roughness, nonuniform distributions of the roughness, and anisotropic properties. The rough surface is modeled as a distribution of dipole and monopole sources on the flat surface. Also Tolstoy (1979, 1981, 1984) utilizes the Biot model to study various phenomena related to the rough surfaces, such as scattering of spherical pulses, energy transmission into shadow zones, and boundary waves caused by the surface roughness. However, the present work is limited to the far field effects of the reflected signal.

II. THEORY

In this paper, the most relevant part of the work by Biot is the representation of a rough surface as a distribution of image sources below the flat surface image source. As long as the more general boundary conditions, as in Biot (1968), have the same linear form as the boundary condition in Biot (1957), i.e.,

$$\frac{\partial\phi}{\partial z}=-A\frac{\partial^2\phi}{\partial z^2}-Bk^2\phi, \tag{2}$$

with any real A and B, the logic presented in Biot's first paper (1957) can be applied. For hemispherical bosses, $A=B=1/2\sigma$, where $\sigma=2\pi Na^3$, N is the number of bosses per unit area, and a is the radius of the bosses. As shown in Biot (1968), representing the rough surface with monopoles and dipoles, instead of only dipoles as in Biot (1957), does not change the form of the boundary condition. It is possible to model interacting bosses and bosses of different shapes by only changing A and B.

This approach has some limitations. The modeled wavelength must be larger than the dimensions of the roughness. In addition, the surface is assumed to be hard. Nonuniform roughness and anisotropic roughness require different boundary conditions (see, e.g., Biot, 1968).

In the following, Biot's theory is briefly reviewed. The same derivation can be found in Biot (1957), but here the boundary conditions are slightly more general. The theoretical contribution of this paper is to explicitly derive the exponential decay approximation in the time domain assuming the given boundary condition.

The total sound field can be expressed as a sum of three components

$$\phi=\varphi_s+\varphi_i+\varphi, \tag{3}$$

where φ_s is the incident field emitted by the source, φ_i is the field reflected specularly, or equivalently emitted by the image source, and φ is the field caused by the roughness of the surface.

The source is assumed to be a monopole

$$\varphi_s=D\frac{e^{-ikR_s}}{R_s}, \tag{4}$$

where D is the magnitude of the source, and R_s is the distance from a surface point ($z=0$) to the source. It can be divided into components

$$\begin{aligned} R_s&=\sqrt{r^2+(z-h)^2},\\ r^2&=x^2+y^2, \end{aligned} \tag{5}$$

where r is the distance along the flat surface to the point closest to the source on the surface and h is the perpendicular distance from the source to the surface. The image source is defined similarly, but h is replaced with $-h$. Figure 1 illustrates the setup.

The source (and image source) can be expressed with the Sommerfeld integral as

$$\varphi_s=D\int_0^\infty\frac{1}{\mu}e^{-\mu|z-h|}J_0(lr)l\mathrm{d}l, \tag{6}$$

where $\mu=\sqrt{l^2-k^2}$ and J_0 is the zeroth order Bessel function of the first kind. Thus, when $-h<z<h$, the sum of the incident and ideally specularly reflected field is

$$\varphi_s+\varphi_i=D\int_0^\infty\frac{1}{\mu}J_0(lr)e^{-\mu h}(e^{\mu z}+e^{-\mu z})l\mathrm{d}l. \tag{7}$$

To solve φ, the scattered field is written as a similar kind of integral with an unknown spectral function $F(l)$

$$\varphi=\int_0^\infty\frac{1}{\mu}F(l)J_0(lr)e^{-\mu(z+h)}l\mathrm{d}l. \tag{8}$$

This is a solution to the wave equation, Eq. (1), and it fulfills the Sommerfeld radiation condition in the positive half-space above the specular image source. Then, the total field, as in Eq. (3), is calculated from Eqs. (7) and (8). This is substituted in the boundary condition, Eq. (2), and setting $z=0$ yields

$$F(l)=-2D\frac{(A-B)\mu^2+Bl^2}{(A-B)\mu^2-\mu+Bl^2}. \tag{9}$$

The result can be interpreted by considering the total reflected field

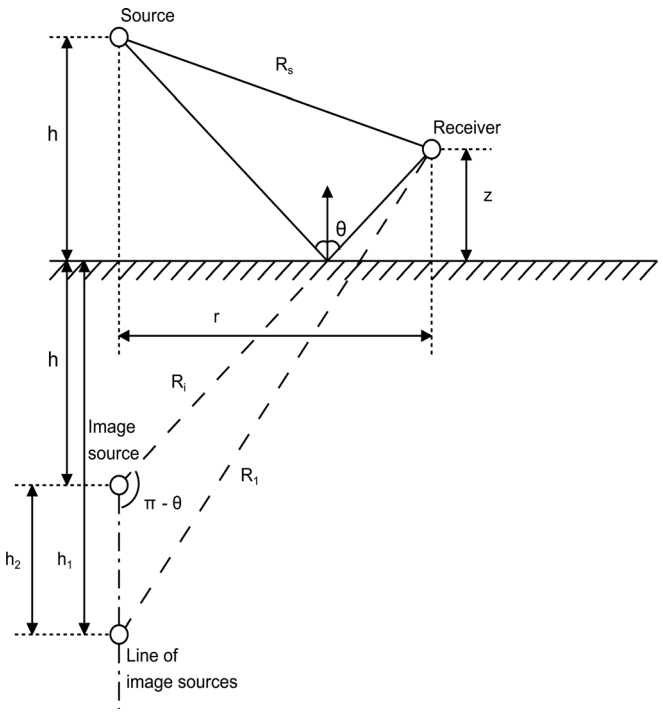

FIG. 1. Sound from a source is reflected via a rough plane to a listener. The specular image source as well as a line of image sources distributed below it are shown. The *xy*-plane is along the horizontal direction and the *z*-axis is along the vertical direction.

$$\begin{aligned}\varphi_i + \varphi &= D\int_0^\infty \frac{1}{\mu} J_0(lr) e^{-\mu(z+h)} l\mathrm{d}l \\ &\quad + \int_0^\infty \frac{1}{\mu} F(l) J_0(lr) e^{-\mu(z+h)} l\mathrm{d}l \\ &= D\int_0^\infty \frac{1}{\mu} G(l) J_0(lr) e^{-\mu(z+h)} l\mathrm{d}l, \end{aligned} \tag{10}$$

where

$$\begin{aligned} G(l) &= \frac{\mu + (A-B)\mu^2 + Bl^2}{\mu - (A-B)\mu^2 - Bl^2} \\ &= \frac{\mu + A\mu^2 + Bk^2}{\mu - A\mu^2 - Bk^2}. \end{aligned} \tag{11}$$

Equation (10) can be split into three parts by presenting $G(l)$ as partial fractions

$$G(l) = -1 + \frac{C_1}{\mu + \mu_1} + \frac{C_2}{\mu + \mu_2}, \tag{12}$$

where

$$\begin{aligned} \mu_1 &= -\frac{1}{2A}\left(1 + \sqrt{1 - 4ABk^2}\right), \\ \mu_2 &= -\frac{1}{2A}\left(1 - \sqrt{1 - 4ABk^2}\right), \\ C_1 &= 1 + \frac{1}{\sqrt{1 - 4ABk^2}}, \\ C_2 &= 1 - \frac{1}{\sqrt{1 - 4ABk^2}}. \end{aligned} \tag{13}$$

It is clear that the first term of $G(l)$ corresponds to the negative image source. The two other terms, which produce integrals of the form

$$\varphi_1 = DC_1 \int_0^\infty \frac{1}{\mu}\frac{1}{\mu + \mu_1} J_0(lr) e^{-\mu(z+h)} l\mathrm{d}l \tag{14}$$

are examined next. Formulas are shown only for index 1, but the same logic applies to index 2. First, an image source, at depth h_1 below the reflecting plane is written as

$$\begin{aligned} \frac{e^{-ikR_1}}{R_1} &= \int_0^\infty \frac{1}{\mu} J_0(lr) e^{-\mu(z+h_1)} l\mathrm{d}l, \\ R_1 &= \sqrt{r^2 + (z+h_1)^2}. \end{aligned} \tag{15}$$

It is possible to multiply both sides with $e^{-\mu_1 h_1}$ yielding

$$e^{-\mu_1 h_1}\frac{e^{-ikR_1}}{R_1} = \int_0^\infty \frac{1}{\mu} J_0(lr) e^{-\mu z} e^{-(\mu+\mu_1)} h_1 l\mathrm{d}l. \tag{16}$$

This can be integrated with respect to h_1 from h to ∞

$$\begin{aligned} \int_h^\infty e^{-\mu_1 h_1}\frac{e^{-ikR_1}}{R_1}\mathrm{d}h_1 &= \int_0^\infty \frac{1}{\mu} J_0(lr) e^{-\mu z} l\mathrm{d}l \int_h^\infty e^{-(\mu+\mu_1)h_1}\mathrm{d}h_1 \\ &= e^{-\mu_1 h}\int_0^\infty \frac{1}{\mu}\frac{1}{\mu+\mu_1} J_0(lr) e^{-\mu(z+h)} l\mathrm{d}l. \end{aligned} \tag{17}$$

The last line resembles Eq. (14). Thus, multiplying this equation (without the intermediate form) with $DC_1 e^{\mu_1 h}$ gives

$$DC_1 \int_h^\infty e^{-\mu_1(h_1 - h)}\frac{e^{-ikR_1}}{R_1}\mathrm{d}h_1 = \varphi_1. \tag{18}$$

In other words, the extra two terms in the reflected field can be represented as a continuous distribution of image sources below the specular image source where the amplitude of the image sources is scaled exponentially with depth, i.e., $e^{-\mu_1(h_1 - h)}$.

A. Far field approximation

In the far field, Eq. (18) can be simplified. First, distance R_1 is written with the help of the reflection angle θ and the ideal image source distance R_i by using the law of cosines

$$R_1^2 = R_i^2 - 2R_i(h_1 - h)\cos(\pi - \theta) + (h_1 - h)^2. \tag{19}$$

Then R_1 is written as

$$R_1 = R_i\sqrt{1 + 2\tfrac{h_2}{R_i}\cos\theta + \tfrac{h_2^2}{R_i^2}}, \tag{20}$$

where $h_2 = (h_1 - h)$.

Since the most significant contributions from the line of image sources as in Eq. (18) come when h_2 is small, an assumption is made that $h_2/R_i \ll 1$ in the far field.

The expression below the square root is close to unity and first order Taylor series approximation is used

$$R_1 \approx R_i\left(1+\frac{h_2}{R_i}\cos\theta+\frac{h_2^2}{2R_i^2}\right). \tag{21}$$

Since $h_2/R_i \ll 1$, it is assumed that $h_2^2/R_i^2 \approx 0$ and the second order term is discarded

$$R_1 \approx R_i + h_2\cos\theta. \tag{22}$$

Substitution of Eq. (22) into Eq. (18) yields

$$\varphi_1 = DC_1\int_0^\infty e^{-\mu_1 h_2}\frac{e^{-ik(R_i+h_2\cos\theta)}}{R_i+h_2\cos\theta}\mathrm{d}h_2. \tag{23}$$

Further assuming that $1/(R_i+h_2\cos\theta)\approx 1/R_i$ in the far field, the integral can be rearranged and solved

$$\begin{aligned}\varphi_1 &\approx DC_1\frac{e^{-ikR_i}}{R_i}\int_0^\infty e^{-(\mu_1+ik\cos\theta)h_2}\mathrm{d}h_2\\ &= \frac{DC_1}{\mu_1+ik\cos\theta}\frac{e^{-ikR_i}}{R_i}.\end{aligned} \tag{24}$$

Then the total reflected field as in Eqs. (10) and (12) becomes

$$\begin{aligned}\varphi_i+\varphi &= D\left(-1+\frac{C_1}{\mu_1+ik\cos\theta}+\frac{C_2}{\mu_2+ik\cos\theta}\right)\frac{e^{-ikR_i}}{R_i}\\ &= DS(k)\frac{e^{-ikR_i}}{R_i},\end{aligned} \tag{25}$$

where

$$S(k) = \frac{i\cos\theta-(A\cos^2\theta-B)k}{i\cos\theta+(A\cos^2\theta-B)k}. \tag{26}$$

Obviously, the magnitudes of the numerator and denominator in the expression $S(k)$ multiplying the source are equal. Basically, this means that there is a frequency- and angle-dependent phase shift while the intensity is the same as for the ideal reflection. Energy is thus preserved as it should be, but the reflection is incoherent.

B. Time domain response

In the following, given an impulse-like source signal, the shape of the reflected signal is examined in the time domain. Beginning with Eq. (25), the time domain signal is obtained by Fourier transform. First, the phase shift factor is divided into two parts

$$\begin{aligned}S(k) &= \frac{i\cos\theta}{i\cos\theta+(A\cos^2\theta-B)k}-\frac{(A\cos^2\theta-B)k}{i\cos\theta+(A\cos^2\theta-B)k}\\ &= S_1(k)+S_2(k).\end{aligned} \tag{27}$$

The inverse Fourier transform of this is denoted as $s(t)=s_1(t)+s_2(t)$. The transform is simple

$$s_1(t) = qH(t)e^{-qt}, \tag{28}$$

where $H(t)$ is the Heaviside step function and

$$q = \frac{c\cos\theta}{B-A\cos^2\theta}. \tag{29}$$

It is easy to see that $S_2(k)=S_1(k)-1$. Thus the inverse Fourier transform becomes

$$s_2(t) = qH(t)e^{-qt}-\delta(t), \tag{30}$$

where $\delta(t)$ is the Dirac delta function. The total field is thus

$$s(t) = 2qH(t)e^{-qt}-\delta(t). \tag{31}$$

Integrating $s(t)$ from zero to infinity produces unity, which is an indication that energy is preserved as it should be.

The approximation presented above leads to a model where the rough surface produces an exponentially decaying tail in the time-domain response. This is utilized in the following as the practical aspects of modeling multiple rough surfaces in a room are considered.

III. MODELING WITH BEAMTRACER

The rough surface model presented above can be used with any geometric acoustic algorithm that creates image sources. However, a beam tracing algorithm is considered in this paper because of its efficiency (Funkhouser *et al.*, 2004).

Beam tracing is an algorithm for finding specular reflection paths in a room. A beam tracer finds the same set of valid image sources as the basic image source method (Allen and Berkley, 1979; Borish, 1984). However, ideally, it does not have to separately validate the paths since only valid paths are generated. This is achieved by tracing volumes that must contain the valid paths. These volumes are called beams.

In an image source method, the number of all image sources grows exponentially as the reflection order increases. By limiting consideration to only valid image sources at each reflection order, beam tracing effectively reduces the base number of the exponentiation.

There are versions of the beam tracer algorithm that do not construct accurate beams and thus require path validation (see, e.g., Laine *et al.*, 2009). They can still be faster than accurate beam tracers when modeling early reflections since they can avoid the cost of accurate volume clipping and use special optimization techniques to avoid most of the validation costs.

The beams are cones that are defined with the help of image sources (or the source at first) and polygons that constitute the room model. Each image source acts as an apex point. Planes that contain the image source and edges of the polygon bound the volume. The beams intersect some of the polygons that define the room. They are split such that the intersection areas with each of the polygons become defining polygons for the next level of beams. The beams are stored in a hierarchical tree structure, where the split beams are children of the original beams. By finding in which beams the receiver position lies, it is possible to construct specular reflection paths by traversing the tree upward.

A. Visibility issues

The challenge is to adapt the beam tracing algorithm to the rough surface model, where, instead of a single image

source, there is a line of image sources. Figure 2 illustrates this in two dimensions. Obviously, the beams are different for image sources at different distances below the reflecting plane.

The image source lines can also be reflected like the image sources. However, when reflected several times via non-parallel planes, the lines become areas, and the areas become volumes bounded by more and more planes as the reflection order increases. Tracking these volumes in the beam tracing algorithm becomes cumbersome. A reasonable approximation is to consider only those image sources that are near the specular image source. There are two reasons for this: (i) amplitude of the image sources decays exponentially when moving away from the specular image source, and (ii) many of the higher order non-specular image sources are invalid, since they correspond to reflection paths that are outside the beams. Thus, contributions of the image source far from the specular image source can be neglected. This is in line with the approximations made in Sec. II A.

The model is simplified such that only the specular image sources are calculated in the beam tracer. However, the impulse response corresponding to the reflection is not an impulse, but the impulse is followed by a rapidly decaying tail of reflections which corresponds to the contributions from the line of image sources. As shown in Sec. II B, that tail has the shape of an exponential function.

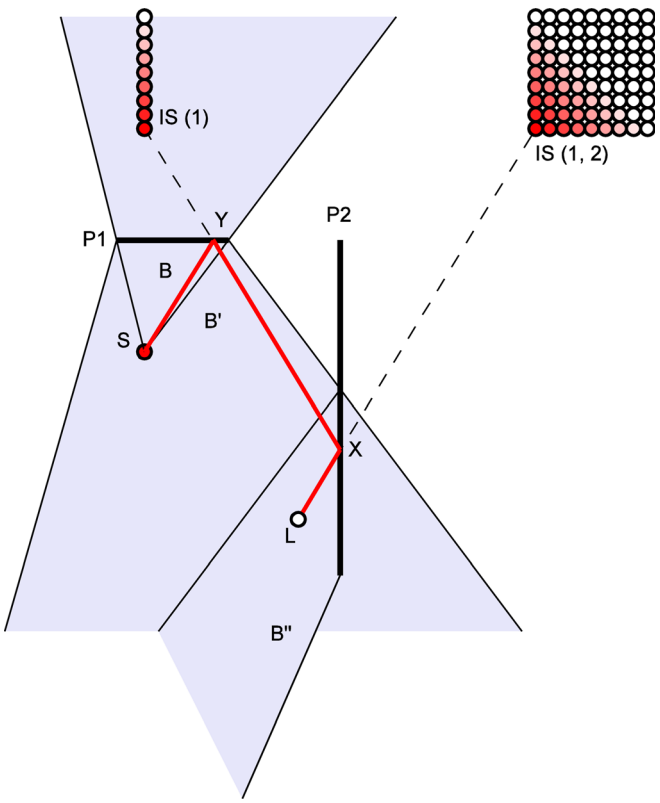

FIG. 2. (Color online) Source S produces a second-order reflection to listener L via polygons $P1$ and $P2$. The reflection path is the thick line. Beam tracer has created beam B defined by source S and polygon $P1$, beam B' which is beam B reflected at polygon $P1$, and beam B'' which is beam B' reflected at polygon $P2$. The listener must be inside the beams for there to be a valid reflection path. Image source $IS(1)$ is source S mirrored with polygon $P1$ and image source $IS(1,2)$ is image source $IS(1)$ mirrored with polygon $P2$. The lines of image sources are illustrated with a finite number of discrete sources, although in reality the distributions are continuous and continue to infinity.

B. Modeling energy vs pressure

The beam tracing model presented here calculates the room responses with energies in time domain. Using complex pressures would be possible if the sampling rate of the room impulse response were infinite. However, with non-infinitesimal sample sizes, there is the possibility that two reflections arrive at different times but fall into the same sample. This causes errors when those contributions are summed up since energy is not preserved. Using energy responses instead of complex impulse responses avoids this problem since energy is well-defined for time intervals, and thus summing up contributions from different reflections into a single sample is physically correct.

The downside of modeling with energies is that phase information is effectively lost. The phase shifts introduced by the rough surfaces still affect the outcome of the computation through the exponential decay curves. Otherwise the limitations of geometric acoustic modeling apply.

The shape of the decay curve is still exponential when modeling energies since energy is proportional to the square of the pressure, and the square of an exponential function is still an exponential function, but with an exponent twice as large.

C. Multiple reflections

In practical modeling applications an efficient handling of higher order reflections is preferred. Based on the theory revised in the previous section, a single reflection is assumed to produce an exponentially decaying tail of reflections after the specular reflection. The decay can be modeled with the help of an enveloping energy function, i.e.,

$$f_i(t) = \begin{cases} R_i e^{-a_i t} & \text{for } t \geq 0 \\ 0 & \text{for } t < 0, \end{cases} \tag{32}$$

where $f_i(t)$ is the time-dependent energy curve, R_i is the reflection coefficient, and a_i is the decay coefficient, all of which for material indexed i. Here, a_i is directly proportional to the factor q as in Eq. (29).

The coefficient can be calculated with the theory or approximated from measured data. Given an impulse response of a reflection from a rough surface, the approximation can be performed as follows. An impulse response is element-wise squared and integrated as advised by Schroeder (1965) in the case of room reverberation time calculation. Analogically, a single reflection can be characterized by a local reverberation time. The decay coefficient is related to the local reverberation time, obtained by fitting a line to the Schroeder-integrated energy curve corresponding to the measured impulse response, as follows:

$$a_i = -\frac{1}{T_{60,i}} \ln(10^{-6}). \tag{33}$$

Local reverberation times obviously depend on the scale of the roughness and the incident angle.

When several reflections occur, their combined effect on the impulse can be calculated as a convolution of the exponential functions corresponding to the reflecting surfaces. The form of the convolution of exponential functions depends on $a_i, i \in N^+$. If they are all different, i.e., $a_i \neq a_j$, $i \neq j$, the convolution is calculated as follows:

$$f_1(t) * f_2(t) * \cdots * f_n(t) = \begin{cases} \sum_{i-1}^{n} \frac{\prod_{j=1}^{n} R_j}{\prod_{j=1, j\neq i}^{n} (a_j - a_i)} e^{-a_i t} & \text{for } t \geq 0 \\ 0 & \text{for } t < 0. \end{cases} \quad (34)$$

If they all have the same value, i.e., $a_i = a \ \forall i$, the result is

$$f_1(t) * f_2(t) * \cdots * f_n(t) = A(n,a) g(t,n,a) = \begin{cases} \frac{\prod_{i=1}^{n} R_i t^{n-1}}{(n-1)!} e^{-at} & \text{for } t \geq 0 \\ 0 & \text{for } t < 0. \end{cases} \quad (35)$$

This is a gamma function scaled with the reflection coefficients. The gamma function can be denoted as $g(t,n,a)$, where n is the order of the gamma function that corresponds to the reflection order of the path, and $A(n,a)$ is a scaling function such that the function can be written in the standard form

$$g(t,n,a) = \frac{a^n}{\Gamma(n)} t^{n-1} e^{-at}, \quad (36)$$

where $\Gamma(n) = (n-1)!$ since n is a positive integer. Thus,

$$A(n,a) = \frac{\prod_{i=1}^{n} R_i}{a^n}. \quad (37)$$

There is an analytic solution for the convolution in Eq. (34) where the a's are a mixture of the same and different values (Akkouchi, 2008). However, the gamma function is faster to calculate and an approximation is proposed here. Since the a's are close to each other in typical cases, their geometric average is used for calculating the gamma function. This approximation leads to a small error, which is examined next.

D. Validation of the approximation

Figure 3(a) shows a case where exponential functions are convolved. The corresponding decay times are typical for a surface with roughness sizes of a few centimeters. The convolution is performed exactly and also with the gamma approximation. It can be seen that the approximating curve is slightly higher at the peak level and its tail then decreases more rapidly than the tail of the curve for the exact solution. The same phenomenon can be seen in the case of three convolved exponential functions as in Fig. 3(b).

The total error in the approximation is relatively small. The normalized root mean square errors in the test cases mentioned above are 0.0289% and 0.1286% for the two response and three response convolutions, respectively. The error increases when the local reverberation times (and thus a's) differ much from each other. When there are more convolutions, the errors accumulate, which can be seen in Fig. 3(c). Normalized root mean square error is already 0.9954% in this case. However, these correspond to reflections via multiple surfaces and later in the reverberant tail of the response, where single reflections are not that important.

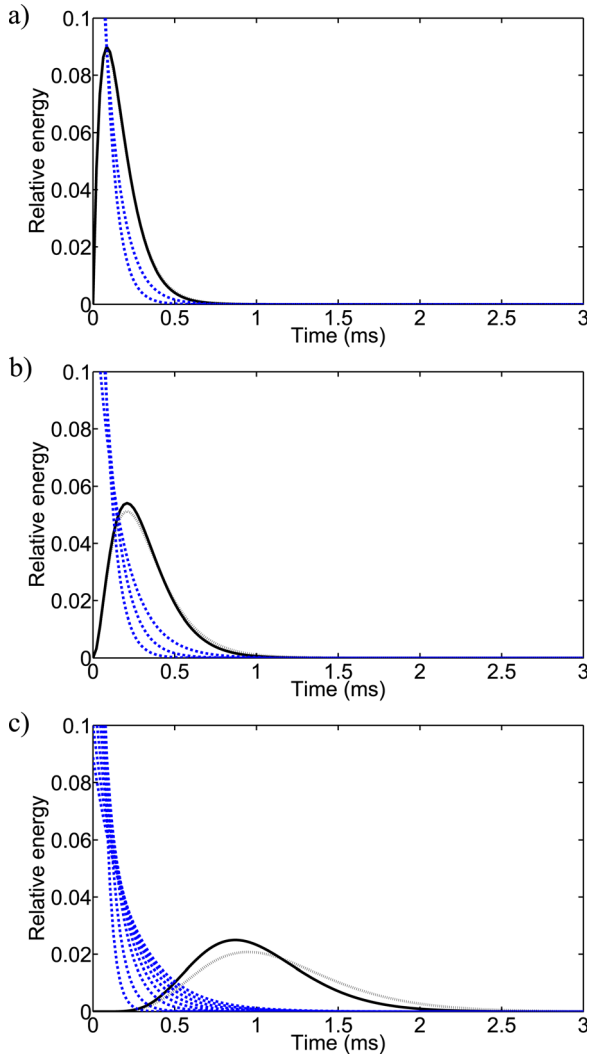

FIG. 3. (Color online) The dotted curves are produced with exact convolution and the solid ones with the gamma function approximation. (a) Convolution of two exponential functions with $T_{60,1} = 0.8$ ms and $T_{60,2} = 1.2$ ms (dashed curves). (b) Convolution of three exponential functions with $T_{60,1} = 0.8$ ms, $T_{60,2} = 1.2$ ms, and $T_{60,3} = 1.8$ ms (dashed curves). (c) Convolution of eight exponential functions. The local reverberation times are 0.5, 0.8, 1.2, 1.5, 1.8, 2.1, 2.4, and 2.7 ms (dashed curves).

E. Modified beam tracing algorithm

The constructed reflection model can easily be incorporated into a beam tracing algorithm. The algorithm calculates the reflection paths as usual, and records the surfaces that are hit along each path. In a regular beam tracing algorithm each reflection path corresponds to a peak in the impulse response. The time of the peak equals the path length, r, divided by the speed of sound. The amplitude of the peak is multiplied by $1/r$, when operating with pressures, and by all the reflection coefficients of the surfaces hit along the path.

When using the reflection model described above, each reflection path corresponds not to a peak, but to an

attenuating series of peaks in the impulse response since the reflections are spreading in time. To get the attenuating series of peaks for a reflection path, the enveloping function, i.e., the function that determines the attenuation, must be calculated. This is calculated in energy, not in pressure. This time-dependent energy function is calculated as a convolution of exponentially decaying energy functions, which correspond to the time-spreading of the reflections along the path. The function can be approximated with the gamma function as explained in Sec. III C.

After the enveloping energy function has been calculated, the impulse response is obtained from it as in Kuttruff (1993). The response must follow the enveloping function and have the correct energy. One approach would be to take white noise and multiply it with the envelope.

However, in the presented implementation, a computationally more efficient technique is used. Instead of introducing randomness into amplitudes, it is added into arrival times of reflections. The enveloping function is sampled with the stratified sampling approach such that there is one random sample per a small time window. The magnitude of each sample is adjusted so that it corresponds to the energy of the function integrated over the time window. The integration of the energy over the time window is performed numerically with the trapezoid rule.

Eventually, summing up contributions from all the reflection paths yields a room impulse response that models the time-dependent nature of the wall reflections.

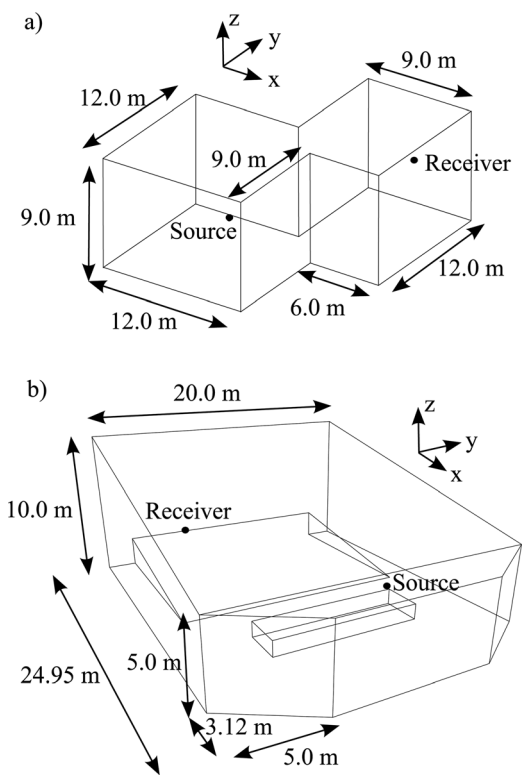

FIG. 4. Models used in the simulation (a) double cube, and (b) auditorium. In (a) the source is at position (9.0; 3.0; 5.4) m and in (b) at position (17.36; 13.76; 2.0) from the leftmost bottom corner. In (a) the receiver is at position (15.0; 18.0; 5.4) m and in (b) at position (4.1; 5.08; 3.3) from the leftmost bottom corner.

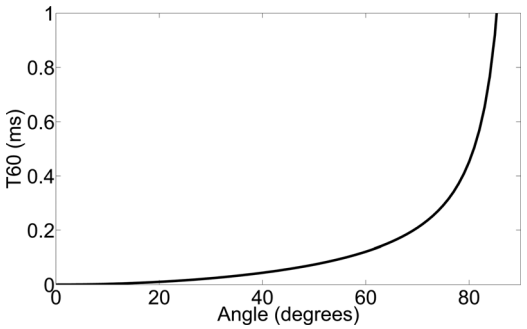

FIG. 5. Local reverberation times used in reflection modeling for a single rough surface.

The proposed procedure does not increase the run time of the beam tracing algorithm itself, but only adds a post-processing step that takes little additional time since evaluating the analytic expressions of Eq. (35) is straightforward. Thus, the proposed modeling approach is much faster than calculating the convolutions of the reflected impulse responses during the beam tracing process.

F. Discussion with examples

The effects of the time spreading model can be easily seen by showing an example. The purpose of this discussion is not to validate the model as such because the theoretical work is based on solid physical foundation within the assumptions given.

The proposed extension to the beam tracing model was tested with two simple geometries. The three-dimensional polygon models are quite simple since the emphasis is on modeling materials and simple models allow higher order reflections to be modeled. The first geometry consists of two cubic rooms that are overlapped over one edge. The other geometry is a large auditorium. The dimensions of the model and the source and receiver positions are shown in Fig. 4.

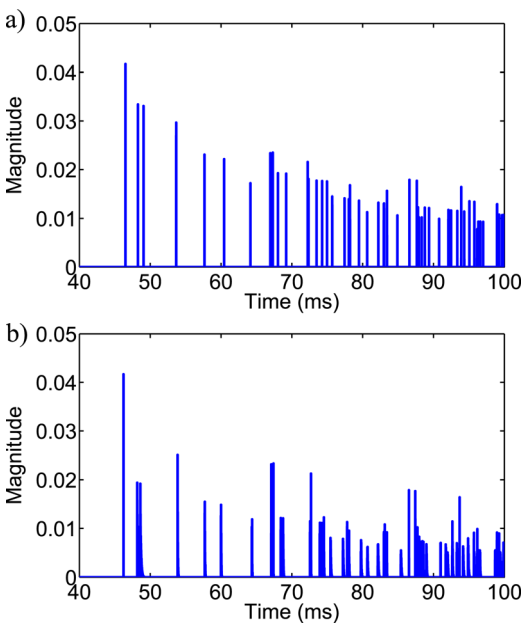

FIG. 6. (Color online) Responses calculated with (a) traditional beam tracing and (b) beam tracing spreading the reflections in time.

TABLE I. Standard room acoustics parameters (ISO, 2009) both for traditional beam tracing and the presented algorithm in the double cube model. The parameters are reverberation time (T_{30}), early decay time (EDT), strength (G), clarity (C_{80}), definition (D_{50}), center time (T_s), and lateral freedom (LF). The differences between the parameter values simulated with the algorithms are shown so that they can be directly compared with the subjected just noticeable difference (JND) values.

Parameter	Traditional	Presented	Difference	JND
T_{30}	0.5946 s	0.5870 s	1.3%	5%
EDT	0.7038 s	0.7129 s	1.3%	5%
G	7.3984 dB	7.5098 dB	0.1114 dB	1 dB
C_{80}	3.2555 dB	2.9789 dB	0.2766 dB	1 dB
D_{50}	54.17%	52.96%	1.21%	5%
T_s	54.8 ms	56.1 ms	1.3 ms	10 ms
LF	35.63%	35.46%	0.17%	5%

The materials were set in both cases so that the absorption coefficient is constant $\alpha = 0.3$. The number was chosen to get reasonable reverberation times, while the emphasis is on modeling time spreading. The angle dependent decay times were calculated from Eqs. (31) and (33) assuming $a_i = 2q$ because energy is related to the square of the pressure. The dimensions of the roughness were chosen to be 0.01 m. Figure 5 shows the local reverberation times calculated in this case. For the model to be valid, the assumption $ka \ll 1$ must be true. Here, the model is valid up to about 500 Hz. Above that frequency, a different scattering model must be used for accurate results.

The simulation was run with both the traditional beam tracing and the beam tracing with reflections spreading in time. The beam tracing was performed up to eighth order after which the late reverberation was modeled with the acoustic radiance transfer technique (Siltanen *et al.*, 2007). Thus, the late reverberation tail was the same regardless of the version of beam tracing used.

The early parts of the resulting impulse responses in the auditorium model are shown in Fig. 6. Tables I and II list standard room acoustic parameters calculated from the responses in the double cube model and auditorium model, respectively.

The acoustics parameters and energy curves, calculated from the impulse responses produced with the traditional and the proposed beam tracing, are very similar. All the acoustics parameters are within the just noticeable difference limens. However, informal listening tests reveal clear differences between the responses convolved with a dry sound stream. Lokki *et al.* (2011) showed that this should be the case. Further tests are required to confirm the perceptual significance of incorporating time spreading in specular reflection modeling.

TABLE II. Standard room acoustics parameters (ISO, 2009) both for traditional beam tracing and the presented algorithm in the auditorium model. The parameters are the same as in Table I. The differences between the parameter values simulated with the algorithms are shown so that they can be directly compared with the subjected just noticeable difference (JND) values.

Parameter	Traditional	Presented	Difference	JND
T_{30}	0.8002 s	0.7961 s	0.5%	5%
EDT	0.7721 s	0.7715 s	0.1%	5%
G	9.9496 dB	10.0102 dB	0.0606 dB	1 dB
C_{80}	6.3393 dB	5.9287 dB	0.4106 dB	1 dB
D_{50}	60.41%	57.45%	2.96%	5%
T_s	53.5 ms	57.8 ms	4.3 ms	10 ms
LF	28.15%	30.39%	2.24%	5%

IV. CONCLUSIONS

A theoretical model for temporally distributed diffuse reflections when $ka \ll 1$ is introduced. A single reflection is assumed to consist of a specular reflection followed by an exponentially decaying tail of non-specular reflections. Higher order reflections, requiring convolutions of the single reflection responses, are modeled with gamma functions. In the beam tracer, it is only necessary to record the local reverberation times of the reflecting room surfaces. Those can be used for calculating the decay curve which acts as an envelope for the noise-like reflections.

Previous room acoustic models offer representations for diffuse reflections with energies, but the use of Biot's theory of reflections from rough surfaces makes it possible to model diffuse reflections with pressures.

ACKNOWLEDGMENTS

The research leading to these results has received funding from the Academy of Finland, Project Nos. 138780 and 218238, and ERC Grant Agreement No. 203636.

Akkouchi, M. (**2008**). "On the convolution of exponential distributions," J. Chungcheong Math. Soc. **21**, 501–510.
Allen, J. B., and Berkley, D. A. (**1979**). "Image method for efficiently simulating small-room acoustics," J. Acoust. Soc. Am. **65**, 943–950.
Biot, M. A. (**1957**). "Reflection on a rough surface from an acoustic point source," J. Acoust. Soc. Am. **29**, 1193–1200.
Biot, M. A. (**1958**). "On the reflection of acoustic waves on a rough surface," J. Acoust. Soc. Am. **30**, 479–480.
Biot, M. A. (**1968**). "Generalized boundary conditions for multiple scatter in acoustic reflection," J. Acoust. Soc. Am. **44**, 1616–1622.
Borish, J. (**1984**). "Extension to the image model to arbitrary polyhedral," J. Acoust. Soc. Am. **75**, 1827–1836.
Chu, D., and Stanton, T. K. (**1990**). "Application of Twersky's boss scattering theory to laboratory measurements of sound scattered by a rough surface," J. Acoust. Soc. Am. **87**, 1557–1568.
Cox, T. J., Dalenbäck, B.-I., D'Antonio, P., Embrechts, J. J., Jeon, J. Y., Mommertz, E., and Vorländer, M. (**2006**). "A tutorial on scattering and diffusion coefficients for room acoustic surfaces," Acta. Acust. Acust. **92**, 1–15.
Dalenbäck, B.-I. (**1996**). "Room acoustic prediction based on a unified treatment of diffuse and specular reflection," J. Acoust. Soc. Am. **100**, 899–909.
Eckart, C. (**1953**). "The scattering of sound from the sea surface," J. Acoust. Soc. Am. **25**, 566–570.
Funkhouser, T. A., Tsingos, N., Carlbom, I., Elko, G., Sondhi, M., West, J. E., Pingali, G., Min, P., and Ngan, A. (**2004**). "A beam tracing method for interactive architectural acoustics," J. Acoust. Soc. Am. **115**, 739–756.
Gilbert, F., and Knopoff, L. (**1960**). "Seismic scattering from topographic irregularities," J. Geophys. Res. **65**, 3437–3444.
Huopaniemi, J., Savioja, L., and Karjalainen, M. (**1997**). "Modeling of reflections and air absorption in acoustical spaces—A digital filter design approach," in *Proceedings of the IEEE Workshop on Applications of Signal Processing to Audio and Acoustics*, Mohonk, New Paltz, NY.
ISO. (**2009**). ISO 3382-1:2009, "Acoustics—Measurement of room acoustics parameters—Part 1: Performance spaces" (International Standards Organization).

Kuttruff, K. H. (**1993**). "Auralization of impulse responses modeled on the basis of ray-tracing results," J. Audio Eng. Soc. **41**, 876–880.
Laine, S., Siltanen, S., Lokki, T., and Savioja, L. (**2009**). "Accelerated beam tracing algorithm," Appl. Acoust. **70**, 172–181.
Lokki, T., Pätynen, J., Tervo, S., Siltanen, S., and Savioja, L. (**2011**). "Temporal envelope preserving reflections surrounding the listener make engaging acoustics," J. Acoust. Soc. Am. **129**, EL223–EL228.
Ogilvy, J. A. (**1987**). "Wave scattering from rough surfaces," Rep. Prog. Phys. **50**, 1553–1608.
Rayleigh, J. W. S. (**1945**). *The Theory of Sound*, 2nd ed. (Dover, New York), Chap. 272a.
Savioja, L., Huopaniemi, J., Lokki, T., and Väänänen, R. (**1999**). "Creating interactive virtual acoustics environments," J. Audio Eng. Soc. **47**, 675–705.
Schroeder, M. R. (**1965**). "New method of measuring reverberation time," J. Acoust. Soc. Am. **37**, 1187–1188.
Siltanen, S., Lokki, T., Kiminki, S., and Savioja, L. (**2007**). "The room acoustic rendering equation," J. Acoust. Soc. Am. **122**, 1624–1635.
Tolstoy, I. (**1979**). "The scattering of spherical pulses by slightly rough surfaces," J. Acoust. Soc. Am. **66**, 1135–1144.
Tolstoy, I. (**1981**). "Energy transmission into shadow zone by rough surface boundary wave," J. Acoust. Soc. Am. **69**, 1290–1298.
Tolstoy, I. (**1984**). "Smoothed boundary conditions, coherent low-frequency scatter, and boundary modes," J. Acoust. Soc. Am. **75**, 1–22.
Twersky, V. (**1957**). "On scattering and reflection of sound by rough surfaces," J. Acoust. Soc. Am. **29**, 209–225.
Vorländer, M., and Mommertz, E. (**2000**). "Definition and measurement of random-incidence scattering coefficients," Appl. Acoust. **60**, 187–199.